THE JOURNAL OF PHYSICAL CHEMISTRY Letters

Letter

pubs.acs.org/JPCL

Mechanism of Sequential Water Transportation by Water Loading and Release in Single-Walled Carbon Nanotubes

Tomonori Ohba,*[,†] Sei-ichi Taira,[†] Kenji Hata,[‡] and Hirofumi Kanoh[†]

[†]Graduate School of Science, Chiba University, 1-33 Yayoi, Inage, Chiba 263-8522, Japan

[‡]Nanotube Research Center, National Institute of Advanced Industrial Science and Technology (AIST), 1-1-1 Higashi Tsukuba, Ibaraki 305-8565, Japan

Supporting Information

ABSTRACT: Water in carbon nanotubes (CNTs) displays unique behaviors such as ring-like structure formation, anomalous hydrogen bonds, and fast transportation. We demonstrated the structures and stability of water in loading and release processes using a combination of X-ray diffraction analysis and hybrid reverse Monte Carlo simulations. Water formed nanoclusters in water loading, whereas layered structures were formed in water release. The water nanoclusters formed in water loading were well stabilized in CNTs. In contrast, in water release, the water layers were less stable than the water nanoclusters. The significant stabilization of nanoclusters in water loading and the relatively low stability of water layers in water release suggest easy water loading and release through CNTs, providing sequential water transportation through CNTs.

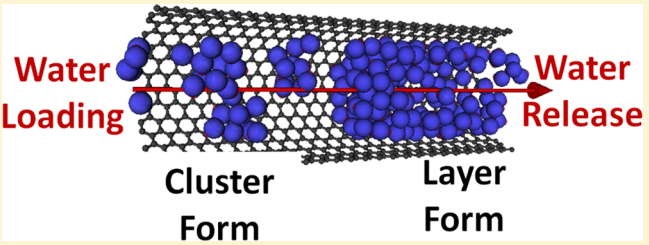

SECTION: Surfaces, Interfaces, Porous Materials, and Catalysis

Nanoconfined water plays a very important role in chemical reactions at solid−liquid interfaces, water transportation through membranes, and controlling biochemical activity. It is therefore necessary to understand the structure and behavior of water in nanospaces. In the liquid state, a water molecule partially forms hydrogen bonds to neighboring water molecules, resulting in the formation of a complex structure. For instance, water has high- and low-density amorphous phases as a result of the formation of water clusters through hydrogen bonding.[1−3] The hydrogen bonds of water confined in nanospaces provide anomalous structure formation and behaviors. Hydrophobic carbon nanospaces have relatively weak interactions with water, so water−water interactions, i.e., hydrogen bonds, should be dominant. Unique water structures and hydrogen bonds have been observed in such nanospaces.[4−7] Byl and co-workers showed anomalous stretching of water in carbon nanotubes (CNTs), using IR spectroscopy.[4] A ring-like water structure has been observed in CNTs.[5,6] Even at low densities, water confined in CNTs forms nanosized clusters at ambient temperature.[7] These unique structure formations are attributed to restriction of hydrogen bonds in such nanospaces. Water gains stability from hydrogen-bonding networks by ring or cluster formation, although water cannot be sufficiently stabilized by interaction with nanospaces.[8] The self-stabilizing mechanism of water in hydrophobic nanospaces is inherently important for water transportation through nanospaces,[9] because water has to be stabilized in nanospaces immediately for loading. Hummer and co-workers showed osmotic water shifts in CNTs, using molecular dynamics simulations.[10,11] Holt and co-workers experimentally demonstrated fast water transportation through CNT membranes.[12] Such water transportation has also been investigated using molecular dynamics simulations.[13−16] Chaban and co-workers demonstrated the dependences of transportation and vapor pressure of water confined in CNTs on tube diameter and temperature; elevation of boiling temperature of water in narrower CNTs as well as the small diffusion coefficient for the extremely narrow CNT.[17−19] However, the mechanism of water loading and release through CNTs remains unclear, although two assembled structures, namely cluster and monolayer-like structures, in two-dimensional nanospaces have been observed in water loading and release processes.[20−22] Moreover, the detailed structure, including the hydrogen-bonding structure, is far from understood, and the mechanisms of water loading and release from CNTs are unclear.

The X-ray diffraction (XRD) technique for molecules confined in nanospaces is a powerful tool for observing molecular structures in nanospaces. Assembled water structures could be evaluated using XRD.[23,24] However, the detailed structure of water confined in nanospaces is difficult to obtain from a typical XRD analysis of a scattering pattern and electron radial distribution functions (RDFs). Monte Carlo simulation is another powerful tool for observing water confined in nanospaces.[25−27] This method provides stable three-dimensional structures of water and therefore hydrogen-bonding networks could also be observed. The main disadvantages of

Received: January 29, 2013
Accepted: March 24, 2013
Published: March 26, 2013

using Monte Carlo simulation are that the molecular structure is not direct proof of the actual structure, and only the most stable structure is obtained. For instance, metastable structures would not be observed from typical Monte Carlo simulations. A combination of XRD analysis and Monte Carlo simulations for obtaining the actual three-dimensional structures of molecules was developed recently to compensate for these disadvantages; this is known as hybrid reverse Monte Carlo (HRMC) simulation.[28−30] HRMC simulations were originally used to obtain the detailed three-dimensional structures of amorphous-like solids. However, the method can also be adapted for the analysis of fluid structures. In this paper, water structures associated with hydrogen bonds in CNTs and their stabilities were evaluated using HRMC simulations as well as electron RDFs, with the aim of understanding the loading and release mechanism of water.

The water vapor adsorption isotherm of CNTs at 303 K is shown in Figure S1 (Supporting Information). In water loading, water filling rates in CNTs were increased with increasing water vapor pressure, or in other words, water was introduced in CNTs by higher water vapor pressure. In contrast, in water release, water amounts in CNTs were decreased by lowering water vapor pressure. The adsorption isotherm has significant adsorption hysteresis in water loading and release. Such adsorption hysteresis of water vapor has been observed in hydrophobic nanospaces.[31−33] Water structures in water loading and release were cluster- and monolayer-like form in slit-shaped nanospaces determined by small-angle X-ray scattering associated with molecular simulation.[21,22,27] The structure transformations in water loading and release were kinetically forbidden in those nanospaces, leading the above different water structure in water loading and release.[33] Those results indicate that different water states and/or structures in CNTs could also be expected in water loading and release. The water structures at 50% filling in water loading and release were evaluated using XRD. Figure S2 shows the XRD patterns for 50% water filling in water loading and release. The XRD patterns for 0% and 100% water filling are also shown for comparison. The XRD intensity increased with increasing amounts of water in the CNTs. The increases in the XRD intensities of water-confined-CNTs compared with those of CNTs in vacuo are a result of water−water and water−carbon scattering. The XRD patterns in water loading and release were significantly different in the scattering parameter range s = 10−17 nm^{-1}; the scattering intensity in water loading was larger than that in water release. The differential XRD patterns of water-confined CNTs and CNTs in vacuo (shown in Figure 1A) were mainly attributed to water structures in the CNTs, as mentioned above. The first XRD peak of liquid water was at approximately 20 nm^{-1}, corresponding to the average water−water distance of 0.32 nm. The average water−water distances in CNTs were longer than that in liquid water: 0.39 nm in water loading, 0.37 nm at full water saturation, and 0.35 nm in water release. Thus, in water loading, the long intermolecular distance decreased with increasing water filling and then further decreased in water release. Here, the longer intermolecular distances of water confined in CNTs relative to those in liquid water are a result of self-assembled structure formation.

The intermolecular distances were directly observed from the electron RDFs, calculated from the differential XRD patterns, as shown in Figure 1B; the electron RDFs unfortunately also include the distance between water and carbon atoms in CNTs, although the correlation between water and carbon atoms is

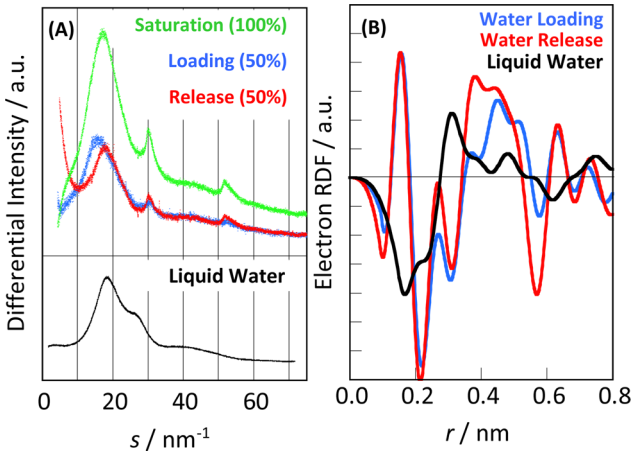

Figure 1. (A) Differential XRD patterns of water confined in CNTs, and XRD pattern of liquid water for comparison. The scattering parameter s is defined as $4\pi \sin\theta/\lambda$ (λ: X-ray wavelength). (B) Electron RDFs of water confined in nanospaces in water loading and release processes. The electron RDF of liquid water is shown for comparison.

inferior. The water−water correlations without the water−carbon correlations could be obtained by HRMC simulation, as described later. The nearest-, second-, and third-neighbor intermolecular distances in liquid water were 0.31, 0.48, and 0.75 nm, respectively. In the case of water confined in CNTs, the first and second peaks were at 0.17 and 0.27 nm. The first peaks were rather shorter than the water−water distance, and were attributed to the OH intermolecular distance, as described later. The second peaks, at 0.27 nm, roughly agree with the intermolecular distance of 0.28 nm for bulk ice. Considerable numbers of hydrogen bonds were therefore formed even at 303 K in CNTs.[7] The broad peaks at around 0.48 nm in water loading and 0.43 nm in water release resulted from the first XRD peaks, indicating the formation of an assembled structure. The correlation between water at longer distances in water loading than in water release might be attributed to cluster formation. The structure in water release was between those in water loading and liquid water, although the intermolecular distance was rather ice-like, shown by the stronger peak at 0.27 nm. Thus, the water structures in water loading and release differed significantly from each other. HRMC simulations were performed for the differential XRD patterns in water loading and release to observe the detailed structures of water in CNTs.

Figure 2A and 2B show comparison of the experimental and HRMC-simulated XRD patterns (see also Figure S3 for liquid water). The XRD patterns in the experiment for liquid water and the HRMC simulation coincide with each other, as shown in Figure S3. The nearest-, second-, and third-neighbor intermolecular distances in the OO distribution were 0.28, 0.46, and 0.66 nm, respectively, which roughly agree with the electron RDFs of liquid water except for the third-neighbor distance; the peaks were at 0.31, 0.48, and 0.75 nm. The OH distribution, which has the peaks at 0.33 nm with the shoulder peak at 0.18 and 0.72 nm, should also contribute to the electron RDF in liquid water. Thus, the shoulder peak at 0.2 nm in the electron RDF and the slight larger distances than those in the OO distribution are a result of the OH distribution. The experimental and HRMC-simulated XRD patterns in water loading and release also coincided well with each other except for a slight difference at around 28 nm^{-1}. The difference might

dx.doi.org/10.1021/jz400218s | J. Phys. Chem. Lett. 2013, 4, 1211−1215

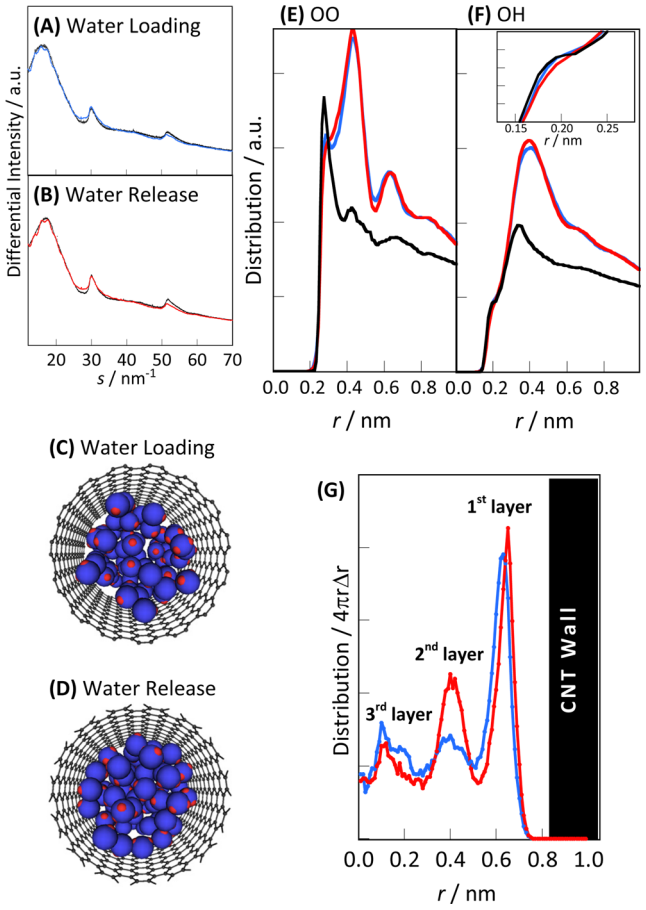

Figure 2. Comparisons of experimental and HRMC-simulated XRD patterns in water loading (A) and release (B). Colored curves: results of HRMC simulations; black curves: experimental results. Snapshots of water in a CNT and water distribution in water loading (C) and release (D). A water molecule is depicted by a blue sphere (oxygen atom) accompanied by two small red spheres (hydrogen atoms). The HRMC-simulated RDFs between OO (E) and OH (F) were obtained using HRMC simulations. The inset figure in the OH distribution is an expansion of the range 0.13−0.28 nm. Distribution of water against distance from the CNT center (G).

be attributed to the assumption of ideal uniform CNT structure in the HRMC simulations, which was apparently different from the actual CNT structure. Here, the scatterings between water and CNTs were also taken into account in the calculations. The partial cross sectional views of water-containing CNTs in water loading and release are shown in Figure 2C and 2D, respectively. Some water molecules were assembled and formed clusters in water loading, whereas in water release, a water layer was observed along the CNT wall. Figure S4 shows the distribution of associated molecular number in water loading and release, calculated from the molecular number within 0.5 nm distance in those snapshots. Water molecules in water loading were a little more associated with each other than those in water release, suggesting that water formed clusters in water loading and layers in water release; those are analyzed in detail later. The simulated RDFs between OO and OH were evaluated from snapshots of the HRMC simulations, as shown in Figure 2E and 2F, respectively. The OO and OH distributions in liquid water were apparently different from the distributions in CNTs. The distributions in liquid water indicated that hydrogen bonds with the nearest-neighbor molecule were unambiguously formed, whereas the correlations with the second- and third-neighbor molecules were weak. On the other hand, long-range correlations were observed for the confined water in both water loading and release. The simulated RDFs for OO have four peaks at around r = 0.30, 0.42, 0.62, and 0.82 nm. No significant peak shifts were observed between water loading and release. However, the nearest-neighbor peak in water loading was relatively significant, the second-neighbor peak was slightly shifted to a longer distance, and the third-neighbor peak was oppositely shifted to a shorter distance. This trend was also observed in the experimental electron RDF shown in Figure 1B. An assembled water structure of size 0.4−0.6 nm was therefore formed in water loading, in agreement with the formation of water nanoclusters reported in previous papers.[7,8] The OH RDFs in water loading and release were very similar to each other: shoulder peaks appeared at the nearest-neighbor OH distance of 0.19 nm, and there were significant peaks at around 0.39 nm. The first peak at 0.19 nm roughly agrees with the peak at 0.17 nm in the experimental electron RDFs in Figure 1B. As the hydrogen-bonding distance of water is 0.18 nm, the water in CNTs formed hydrogen bonds. However, these hydrogen bonds might not be strong, because the second-neighbor OH peaks at 0.39 nm were rather significant. The first peak in water loading was stronger than that in water release, whereas the converse was the case for the second peak. This means that the hydrogen bonds in water loading were stronger than those in water release. The water distributions in Figure 2G clearly show a layered structure in water release; the first, second, and third layers from a CNT wall were respectively positioned at 0.65, 0.40, and 0.1 nm from the center of a CNT. The layered structure was more obvious in water release rather than in water loading, especially for the second layer. The distances between the first layer and the carbon center in a CNT wall in water loading and release, which were 0.35 and 0.37 nm, respectively, were longer than the intermolecular distance evaluated from the collision diameter of 0.327 nm. This is a result of the curvature effect of CNTs, reported elsewhere.[34] The distribution in water loading was relatively broad, as a result of self-assembled clusters. Simply stated, the water in CNTs was in a cluster form in water loading and a layered form in water release.

The water stabilities in water loading and release were evaluated from the sum of the intermolecular interactions, as shown in Figure 3. The total stabilities of water at the first layer from the CNT walls were similar to each other in water loading and release. However, the water stabilities in the inner part of the CNT were obviously different from each other; the water in water loading maintained its stability even in the inner part, whereas the water stability in water release quickly decreased. This is a result of differences of the assembled water structures in water loading and release, because the interaction potentials between water and a CNT are the same for both systems. Thus, in the central part of a CNT, water in water loading was more stabilized by cluster formation than water layers in water release. This indicates that the formation of water clusters in water loading promotes water loading into CNTs, and the water layers in water release are easily extracted from CNTs.

In summary, we described the water structures in CNTs in water loading and release, identified using HRMC simulation combined with XRD. Water nanoclusters were formed in CNTs in water loading, and water layers were formed in water release. Water was significantly stabilized by cluster formation

dx.doi.org/10.1021/jz400218s | J. Phys. Chem. Lett. 2013, 4, 1211−1215

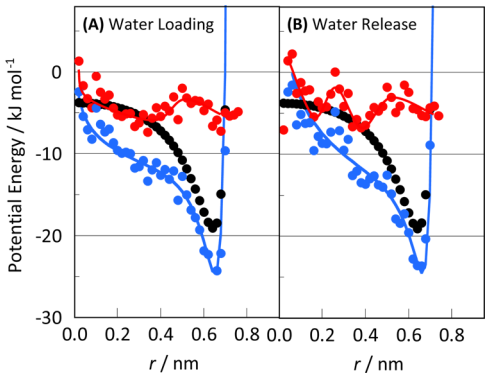

Figure 3. Water stability against distance from a CNT center in water loading and release. Interaction potentials of intermolecular water (red) and water−C atom (black), and the total interaction potentials (blue) along a CNT axis in water loading (A) and release (B).

in water loading. The water stability in water release was less than that in water loading. These stability changes in water loading and release allow sequential water transportation through CNTs. The mechanism of water stability tuning in CNTs provides an understanding of fast water transportation through CNTs.

METHODS

The water vapor adsorption isotherm of CNTs at 303 K was measured after preheating at below 0.01 Pa and at 423 K. The CNTs were evacuated at below 0.1 Pa prior to the XRD measurements. The filling rates of water were controlled as follows (see also Figure S1). Water vapor was loaded into the nanospaces of CNTs at a water vapor pressure of 3.1 kPa (corresponding to 50% filling of the nanospaces), and then at a water vapor pressure of 3.8 kPa (corresponding to 100% filling of the nanospaces), and released until the water vapor pressure was 2.3 kPa (corresponding to 50% filling of the nanospaces). Synchrotron XRDs of water in CNTs were measured at SPring-8 under each of the above conditions, for an accumulation time of 0.5 h and at a wavelength of 0.1000 nm (see more details in the Supporting Information). An HRMC simulation was developed by Opletal et al. and Nguyen et al. for analysis of the detailed structure of amorphous carbon.[28−30] In this study, we adapted the method to analyze the structure of water molecules in CNTs. The method is a combination of the reverse Monte Carlo technique for an XRD pattern and a canonical ensemble Monte Carlo simulation with a controlled weighting factor. The weighting factor was chosen based on two corresponding diffraction patterns, i.e., experimental and simulated patterns, to agree with each other in the reverse Monte Carlo technique, and on high stability of water in CNTs in the canonical Monte Carlo simulation. The calculation cycles consisted of more than 2×10^7 steps. Interaction potential models of water and the carbon of an armchair-type CNT were depicted using a model combining Lennard-Jones and Coulombic potential functions. The CNT diameter was set at 2.0 nm, determined by the N_2 adsorption isotherm at 77 K and transmission electron microscopy, as described in a previous paper.[34] TIP5P model was used for the intermolecular interaction between water, which is relatively well-described structure and density.[35−40] The potential parameters (potential well depth, collision diameter, and partial charge) were as follows: ε_{H2O}/k_B = 80.5 K, σ_{H2O} = 0.312 nm, q_{H2O}/e = ± 0.241 C, ε_C/k_B = 30.14 K, σ_C = 0.3416 nm, and q_C/e = 0 C. The water−carbon interaction was calculated on the basis of the Lorentz−Berthelot mixing rules. Ewald summation was imposed in three directions for the Coulombic interactions between water partial charges. The cutoff length of the potential was set at 5 nm. The unit cell sizes were 100 × 100 × 10 nm^3, with a CNT of length 10 nm, for water confined in a CNT, and 3 × 3 × 3 nm^3 for liquid water. A periodic boundary condition is imposed for three directions in the unit cells. The details of the simulation procedure are shown in the Supporting Information. The structure and stabilized energies of water in carbon nanospaces in Monte Carlo and molecular dynamics simulations using those potential models are consistent with experimental results reported elsewhere.[9,21,27]

ASSOCIATED CONTENT

Supporting Information

Experimental and simulation procedures, water vapor adsorption isotherms of CNTs, XRD patterns of water confined in CNTs and CNTs in vacuo, and XRD patterns of liquid water in experiments and HRMC simulation. This material is available free of charge via the Internet at http://pubs.acs.org.

AUTHOR INFORMATION

Corresponding Author

*E-mail: ohba@pchem2.s.chiba-u.ac.jp.

Notes

The authors declare no competing financial interest.

ACKNOWLEDGMENTS

We thank Dr. J. Kim, Dr. N. Tsuji, and Dr. S. Kohara for their help in recording the XRD data at Spring-8. This work was supported by a Grant-in-Aid for Scientific Research and the Strategic Promotion Program for Basic Nuclear Research, the JGC-S Scholarship Foundation, Promotion of Ion Engineering, Murata Science Foundation, Nippon Sheet Glass Foundation, and the Global COE Program, MEXT, Japan.

REFERENCES

(1) Matsumoto, M.; Saito, S.; Ohmine, I. Molecular Dynamics Simulation of the Ice Nucleation and Growth Process Leading to Water Freezing. *Nature* **2002**, *416*, 409−413.

(2) Head-Gordon, T.; Hura, G. Tetrahedral Structure or Chains for Liquid Water. *Chem. Rev.* **2002**, *102*, 2651−2670.

(3) Bellissent-Funel, M.-C.; Teixeira, J.; Bosio, L. Structure of High-Density Amorphous Water. II. Neutron Scattering Study. *J. Chem. Phys.* **1987**, *87*, 2231−2235.

(4) Byl, O.; Liu, J.-C.; Wang, Y.; Yim, W.-L.; Johnson, J. K.; Yates, J. T. J., Jr. Unusual Hydrogen Bonding in Water-Filled Carbon Nanotubes. *J. Am. Chem. Soc.* **2006**, *128*, 12090−12097.

(5) Koga, K.; Gao, G. T.; Tanaka, H.; Zeng, X. C. Formation of Ordered Ice Nanotubes Inside Carbon Nanotubes. *Nature* **2001**, *412*, 802−805.

(6) Maniwa, Y.; Kataura, H.; Abe, M.; Udaka, A.; Suzuki, S.; Achiba, Y.; Kira, H.; Matsuda, K.; Kadowaki, H.; Okabe, Y. Ordered Water Inside Carbon Nanotubes: Formation of Pentagonal to Octagonal Ice-Nanotubes. *Chem. Phys. Lett.* **2005**, *401*, 534−538.

(7) Ohba, T.; Taira, S.; Hata, K.; Kaneko, K.; Kanoh, H. Predominant Nanoice Growth in Single-Walled Carbon Nanotubes by Water-Vapor Loading. *RSC Adv.* **2012**, *2*, 3634−3637.

(8) Ohba, T.; Kanoh, H.; Kaneko, K. Affinity Transformation from Hydrophilicity to Hydrophobicity of Water Molecules on the Basis of Adsorption of Water in Graphitic Nanopores. *J. Am. Chem. Soc.* **2004**, *126*, 1560−1562.

(9) Ohba, T.; Kaneko, K.; Endo, M.; Hata, K.; Kanoh, K. Rapid Water Transportation through Narrow One-Dimensional Channels by Restricted Hydrogen Bonds. *Langmuir* **2013**, *29*, 1077−1082.
(10) Hummer, G.; Rasaiah, J. C.; Noworyta, J. P. Water Conduction through the Hydrophobic Channel of a Carbon Nanotube. *Nature* **2001**, *414*, 188−190.
(11) Kalra, A.; Garde, S.; Hummer, G. Osmotic Water Transport through Carbon Nanotube Membranes. *Proc. Natl. Acad. Sci. U.S.A.* **2003**, *100*, 10175−10180.
(12) Holt, J. K.; Park, H. G.; Wang, Y.; Stadermann, M.; Artyukhin, A. B.; Grigoropoulos, C. P.; Noy, A.; Bakajin, O. Fast Mass Transport Through Sub-2-Nanometer Carbon Nanotubes. *Science* **2006**, *312*, 1034−1037.
(13) Liu, B.; Li, X.; Li, B.; Xu, B.; Zhao, Y. Carbon Nanotube Based Artificial Water Channel Protein: Membrane Perturbation and Water Transportation. *Nano Lett.* **2009**, *9* (4), 1386−1394.
(14) Li, J.; Gong, X.; Lu, H.; Li, D.; Fang, H.; Zhou, R. Electrostatic Gating of a Nanometer Water Channel. *Proc. Natl. Acad. Sci. U.S.A.* **2007**, *104*, 3687−3692.
(15) Thomas, J. A.; McGaughey, J. H. Reassessing Fast Water Transport Through Carbon Nanotubes. *Nano Lett.* **2008**, *8*, 2788−2793.
(16) Falk, K.; Sedlmeier, F.; Joly, L.; Netz, R. R.; Bocquet, L. Molecular Origin of Fast Water Transport in Carbon Nanotube Membranes: Superlubricity versus Curvature Dependent Friction. *Nano Lett.* **2010**, *10*, 4067−4073.
(17) Chaban, V. V.; Prezhdo, O. V. Water Boiling Inside Carbon Nanotubes: Toward Efficient Drug Release. *ACS Nano* **2011**, *5*, 5647−5655.
(18) Chaban, V. V. Should Carbon Nanotubes Be Degasified before Filling? *Chem. Phys. Lett.* **2010**, *500*, 35−40.
(19) Chaban, V. V.; Prezhdo, V. V.; Prezhdo, O. V. Confinement by Carbon Nanotubes Drastically Alters the Boiling and Critical Behavior of Water Droplets. *ACS Nano* **2012**, *6*, 2766−2773.
(20) Iiyama, T.; Ruike, M.; Kaneko, K. Structural Mechanism of Water Adsorption in Hydrophobic Micropores from in Situ Small Angle X-ray Scattering. *Chem. Phys. Lett.* **2000**, *331*, 359−364.
(21) Ohba, T.; Kaneko, K. Cluster-Associated Filling of Water Molecules in Slit-Shaped Graphitic Nanopores. *Mol. Phys.* **2007**, *105*, 139−145.
(22) Ohba, T.; Kanoh, H.; Kaneko, K. Structures and Stability of Water Nanoclusters in Hydrophobic Nanospaces. *Nano Lett.* **2005**, *5*, 227−230.
(23) Futamura, R.; Iiyama, T.; Hamasaki, A.; Ozeki, S. Negative Thermal Expansion of Water in Hydrophobic Nanospaces. *Phys. Chem. Chem. Phys.* **2012**, *14*, 981−986.
(24) Ohba, T.; Hata, K.; Kanoh, H. Significant Hydration Shell Formation Instead of Hydrogen Bonds in Nanoconfined Aqueous Electrolyte Solutions. *J. Am. Chem. Soc.* **2012**, *134*, 17850−17853.
(25) Striolo, A.; Gubbins, K. E.; Chialvo, A. A.; Cummings, P. T. Simulated Water Adsorption Isotherms in Carbon Nanopores. *Mol. Phys.* **2004**, *102*, 243−251.
(26) Do, D. D.; Do, H. D. A Model for Water Adsorption in Activated Carbon. *Carbon* **2000**, *38*, 767−773.
(27) Ohba, T.; Kaneko, K. Surface Oxygen-Dependent Water Cluster Growth in Carbon Nanospaces with GCMC Simulation-Aided in Situ SAXS. *J. Phys. Chem. C* **2007**, *111*, 6207−6214.
(28) Opletal, G.; Petersen, T.; O'Malley, B.; Snook, I.; Mcculloch, D. G.; Marks, N. A.; Yarovsky, I. Hybrid Approach for Generating Realistic Amorphous Carbon Structure Using Metropolis and Reverse Monte Carlo. *Mol. Simul.* **2002**, *28*, 927−938.
(29) Nguyen, T. X.; Bhatia, S. K. Determination of Pore Accessibility in Disordered Nanoporous Materials. *J. Phys. Chem. C* **2007**, *111*, 2212−2222.
(30) Nguyen, T. X.; Cohaut, N.; Bae, J.-S.; Bhatia, S. K. New Method for Atomistic Modeling of the Microstructure of Activated Carbons Using Hybrid Reverse Monte Carlo Simulation. *Langmuir* **2008**, *24*, 7912−7922.
(31) Rudisill, E. N.; Hacskaylo, J. J.; Le Van, M. D. *Ind. Eng. Chem. Res.* **1992**, *31*, 1122−1130.
(32) Wongkoblap, A.; Do, D. D. Adsorption of Water in Finite Length Carbon Slit Pore: Comparison between Computer Simulation and Experiment. *J. Phys. Chem. B* **2007**, *111*, 13949−13956.
(33) Ohba, T.; Kaneko, K. Kinetically Forbidden Transformations of Water Molecular Assemblies in Hydrophobic Micropores. *Langmuir* **2011**, *27*, 7609−7613.
(34) Ohba, T.; Matsumura, T.; Hata, K.; Yumura, M.; Iijima, S.; Kanoh, H.; Kaneko, K. Nanoscale Curvature Effect on Ordering of N_2 Molecules Adsorbed on Single Wall Carbon Nanotube. *J. Phys. Chem. C* **2007**, *111*, 15660−15663.
(35) Mahoney, M. W.; Jorgensen, W. L. A Five-Site Model for Liquid Water and the Reproduction of the Density Anomaly by Rigid, Nonpolarizable Potential Functions. *J. Chem. Phys.* **2000**, *112*, 8910−8922.
(36) Head-Gordon, T.; Hura, G. Water Structure from Scattering Experiments and Simulation. *Chem. Rev.* **2002**, *102*, 2651−2670.
(37) Hura, G.; Russo, D.; Glaeser, R. M.; Head-Gordon, T.; Krack, M.; Parrinello, M. Water Structure As a Function of Temperature from X-ray Scattering Experiments and *Ab Initio* Molecular Dynamics. *Phys. Chem. Chem. Phys.* **2003**, *5*, 1981−1991.
(38) Lisal, M.; Kolafa, J.; Nezbeda, I. An Examination of the Five-Site Potential TIP5P for Water. *J. Chem. Phys.* **2002**, *117*, 8892−8897.
(39) Brovchenko, I.; Geiger, A.; Oleinikova, A. Liquid−Liquid Phase Transitions in Supercooled Water Studied by Computer Simulations of Various Water Models. *J. Chem. Phys.* **2005**, *123*, 044515.
(40) Vega, C.; Sanz, E.; Abascal, J. L. F. The Melting Temperature of the Most Common Models of Water. *J. Chem. Phys.* **2005**, *122*, 114507.